D. Bruno, A. Frezzotti
Dense Gas Effects in the Rayleigh-Brillouin Scattering Spectra of Sf6
Chemical Physics Letters, Vol. 731, 2019, 136595 (9 pages)
doi:10.1016/j.cplett.2019.136595

Dense Gas Effects in the Rayleigh-Brillouin Scattering Spectra of SF_6

D. Bruno[a,*], A. Frezzotti[b]

[a] *Istituto per la Scienza e Tecnologia dei Plasmi, Consiglio Nazionale delle Ricerche - Via G. Amendola, 122 - 70125 Bari, Italy*
[b] *Dipartimento di Scienze e Tecnologie Aerospaziali, Politecnico di Milano - Via La Masa, 34 - 20156 Milano, Italy*

Abstract

Rayleigh-Brillouin Scattering Spectra of SF_6 are modeled at room temperature in the pressure range $[0.2-5]$ bar and compared to recent experimental measurements [Wang et al. Chem. Phys. Lett. **669** (2017) 137-142]. It is shown that lineshape models that account for density-dependent corrections to the thermodynamic properties provide substantially better agreement than the models assuming an ideal gas model. For intermediate pressures, where a hydrodynamic description of the spectra fails due to kinetic effects, the Enskog-Vlasov kinetic model is shown to reproduce experimental data with good accuracy both at low and high pressure.

Keywords: Rayleigh-Brillouin scattering, SF_6 gas, DSMC simulation, Enskog-Vlason kinetic equation

1. Introduction

The analysis of the power spectrum of spontaneous density fluctuations in fluids provides both an experimental and theoretical tool to investigate their thermodynamic and transport properties [1]. When dealing with gases, laser light scattering experiments [2] allow exploring the characteristics of the fluctuations power spectrum in all flow regimes, from hydrodynamic to collisionless. Theoretical power spectra in the hydrodynamic regime can be obtained by linearized Navier-Stokes equations, either by introducing fluctuating field correlations in the initial state [1] or directly simulating fluctuating stresses and heat flux [3, 4]. In the kinetic regime, spontaneous fluctuations can be analized by the Boltzmann equation [5], linearized around the reference equilibrium state. More often, simpler kinetic models have been successfully adopted [6]. However, the more general Boltzmann equation can be used in combination with

*Corresponding author
Email addresses: domenico.bruno@cnr.it (D. Bruno), aldo.frezzotti@polimi.it (A. Frezzotti)

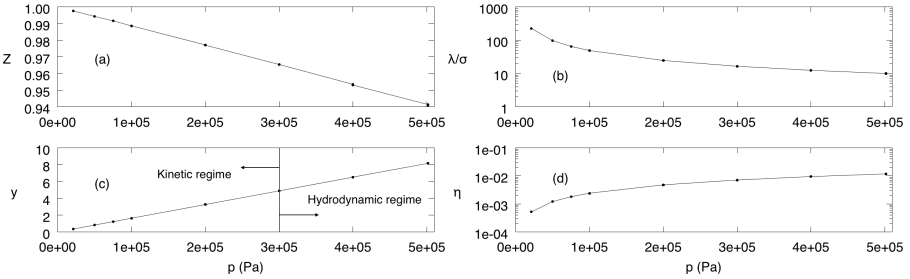

Figure 1: **(a)** SF_6 compressibility $Z = \frac{p(n,T)}{nk_BT}$ as a function of pressure, at $T \approx 296$ K. **(b)** λ/σ as a function of pressure, at $T \approx 296$ K. **(c)** SF_6 rarefaction parameter $y = 1/(k_{sc}\lambda)$, as a function of pressure, at $T \approx 296$ K. The scattering angle θ has been set equal to 89.6° [11]. **(d)** SF_6 reduced density $\eta = \pi\sigma^3 n/6$ as a function of pressure, at $T \approx 296$ K.

the Direct Simulation Monte Carlo method (DSMC) [7] to obtain fluctuations spectra [8, 9, 10] in a dilute gas of arbitrary complexity, not always accessible to kinetic model equations.

The motivation of the present work originates from the experimental power spectra of spontaneous fluctuations in SF_6, described in Ref. [11]. Experiments have been conducted at almost fixed temperature (≈ 296 K), in the pressure range $[0.2 - 5]$ bar and cover all flow regimes from collisionless to hydrodynamic. The companion theoretical analysis has been based on kinetic model equations [6, 12], as well as on a two-temperatures (translational and rotational) hydrodynamic model. The comparison between theoretical and experimental spectra showed discrepancies, the authors attributed to dense gas effects, not accounted for by the adopted models, all based on the dilute gas approximation [11]. Actually, deviations from the ideal behavior are expected to be present in the high pressure experimental conditions, on the ground of a number of physical indicators. Figure 1a presents the plot of SF_6 isothermal compressibility ($T \approx 296$ K) $Z = p(n,T)/(nk_BT)$, showing that the pressure is about 94% of the corresponding ideal value, at 5 bar. The pressure equation of state $p = p(n,T)$ has been obtained from the REFPROP database [13] of the US National Institute of Standards and Technology (NIST), n is the number density and k_B the Boltzmann constant. Further evidence of dense gas effects is provided by plotting the ratio λ/σ of the gas mean free path λ to the molecular size σ as a function of the pressure. As shown in Fig. 1b, the gas undergoes a transition from the dilute to the dense regime while the pressure spans its experimental range. At 5 bar, λ is about ten times the molecular size and the reduced density $\eta = \pi\sigma^3 n/6$, *i.e.* the volume fraction occupied by molecules, amounts to about 1.2%. Therefore, the gas can be considered as moderately or weakly dense. The mean free path has been estimated as $\lambda = v_{th}\mu_s/p$, being $v_{th} = \sqrt{2k_BT/m}$ the equilibrium most probable molecular velocity, m the molecular mass and μ_s the shear viscosity. The molecular diameter σ can be estimated around 5.5 Å from the expression: $\sigma = \sqrt{1/(\sqrt{2}\pi n\lambda)}$.

In agreement with the above considerations, the aim of the present paper is to describe the extension of previous analyses to include dense gas effects, both in the hydrodynamic and kinetic regimes, in order to reduce the gap between theory and experiment. As is usually done in the theoretical treatment of Rayleigh-Brillouin Scattering (RBS), the kinetic and hydrodynamic regimes can be characterized by a non-dimensional parameter. The latter, named y, is defined as the ratio between a wavelength and the mean free path:

$$y = \frac{1}{k_{sc}\lambda}, \quad k_{sc} = \frac{4\pi i_r}{l}\sin(\theta/2). \tag{1}$$

In Eq. (1), k_{sc} is the wave vector of the probed fluctuations (it is the difference between the wave vectors of incoming and scattered laser light), i_r the refraction index, l is the wavelength of the laser and θ the scattering angle. Figure 1c shows the behavior of y as function of p, for $T \approx 296$ K and $\theta = 89.6°$. As a rule of thumb, the value $y = 5$ can be assumed to separate the kinetic from the hydrodynamic regime. As shown in Figure 1c, the *nominal* separation occurs at $p \approx 3$ bar.

Different models have been used to reproduce the measurements in the various regimes. All of them assume that the SF_6 molecule behaves as a rigid rotator having three rotational degrees of freedom and an isotropic inertia tensor. It should be noted that the effect of the vibrational modes is already quite visible from the specific heat at room temperature, since the lowest excited vibrational level has a characteristic vibrational temperature $\theta = 520$ K [14]. However, their relaxation is too slow on the time scale of the experiments. Actually, the vibrational relaxation time is $p\tau_{vib} = 2.22 \cdot 10^{-7}$ atm·s [15], whereas the typical timescale measured in the experiments is in the ns range. Hence, vibrational degrees of freedom are effectively frozen in the experiment, as confirmed by preliminary computations, based on a three temperatures (translational+rotational+vibrational) hydrodynamic model whose results are not reported here.

At the largest pressures, comparisons with experiments have been based on a one-temperature hydrodynamic model described in Section 2. Here, dense gas effects have been taken into account through the non-ideal thermodynamic relationships obtained from the NIST database REFPROP [13]. The kinetic regime has been tackled by two different tools. The first one, described in Section 3, consists in DSMC simulations based on the Boltzmann equation, describing a dilute gas of rigid rotators. The binary collision cross section has been modeled according to the Variable Soft Sphere (VSS) model [16], whereas the energy exchange between internal and translational degrees of freedom has been described by the Larsen and Borgnakke model [17]. Although the Boltzmann equation and DSMC are expected to describe low pressure fluctuations spectra accurately, it is possible that, in principle, there exist a pressure interval where the gas still exhibits both a kinetic and a non-ideal behavior. In order to explore this regime, DSMC simulation based on the Enskog-Vlasov (EV) equation have also been performed. As described in Section 3.1, the EV equation, although approximate, has the capability of describing fluctuations in the whole pressure

range.

Results, described and discussed in Section 4, show that indeed including dense gas effects in the lineshape model leads to a significantly better agreement with the observations in the hydrodynamic regime. In the kinetic regime, DSMC-EV is validated as a viable improvement to DSMC for tackling moderately dense flows; the simple interaction potential considered in the model, however, appears inadequate to correctly reproduce the measured spectra within the small experimental uncertainty; this also underlines, however, the potential of such experiments to provide accurate information on molecular interactions.

2. SF_6 hydrodynamic model

In the hydrodynamic limit, the fluctuation spectra can be analytically computed from the Navier-Stokes-Fourier (NSF) equations, linearized around a given reference equilibrium state [1]. The spectral density of fluctuations is obtained as:

$$\begin{aligned}\frac{S(k,\omega)}{S(k)} &= \frac{\gamma-1}{\gamma}\frac{2\chi k^2}{\omega^2+\chi^2k^4} + \\ &\frac{1}{\gamma}\left[\frac{\Gamma k^2}{(\omega+ck)^2+\Gamma^2k^4}+\frac{\Gamma k^2}{(\omega-ck)^2+\Gamma^2k^4}\right] + \\ &+\frac{k}{\gamma c}\left[\Gamma+(\gamma-1)\chi\right]\times \\ &\left[\frac{\omega+ck}{(\omega+ck)^2+\Gamma^2k^4}-\frac{\omega+ck}{(\omega-ck)^2+\Gamma^2k^4}\right] \end{aligned} \tag{2}$$

In Eq. (2), k is the modulus of the wave vector $\vec{k}$, ω the angular frequency, $S(k,\omega)$ is the density correlation function and $S(k)$ the static structure function [1]. The fluctuation spectrum is defined by the following gas properties, to be computed in the equilibrium reference condition, characterized by the pressure p_0 and temperature T_0:

- $\gamma = c_p/c_v$ is the ratio of constant pressure and constant volume specific heats c_p and c_v.
- c is the adiabatic speed of sound, computed as:

$$c^2 = \left(\frac{\partial p}{\partial \rho}\right)_s = \left(\frac{\partial p}{\partial \rho}\right)_T + \left(\frac{\partial p}{\partial T}\right)_\rho \left(\frac{\partial T}{\partial u}\right)_\rho \left[\frac{p}{\rho^2} - \left(\frac{\partial u}{\partial \rho}\right)_T\right] \tag{3}$$

- $\chi = \frac{\kappa}{\rho c_p}$ is the thermal diffusivity, being κ the thermal conductivity.
- $\nu_l = \frac{1}{\rho}\left(\frac{4}{3}\mu_s + \mu_b\right)$ is a kinematic viscosity constructed with the shear viscosity μ_s and bulk viscosity μ_b; Γ denote the expression $\frac{1}{2}\left[\nu_l + (\gamma-1)\chi\right]$.

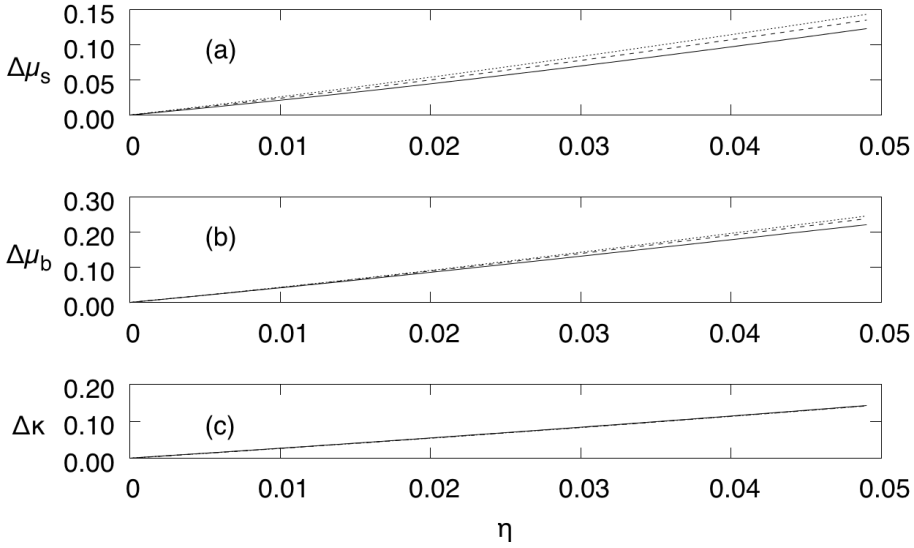

Figure 2: Relative deviations of dense rough sphere gas transport coefficients from the respective ideal gas limits, as a function of the reduced density η; $\Delta x \stackrel{def}{=} (x - x^{(id)})/x$. Solid line: $\kappa = 0.2$; dashed line $\kappa = 0.4$; dashed-dotted line: $\kappa = 0.6$.

Thermodynamic properties of SF_6 in a wide temperature and pressure range can be obtained from the NIST REFPROP database [13]. In particular, all of them are derived from the Helmholtz free energy expression, $a(\rho, T)$, given in Ref. [18] as a function of density and temperature. Care, however, must be exercised when using the database because the free energy expression assumes thermal equilibrium and, consistently, takes into account the vibrational modes contribution. More precisely $a(\rho, T)$ is written as:

$$a(\rho, T) = a^{(0)}(\rho, T) + a^{(r)}(\rho, T), \tag{4}$$

being $a^{(0)}(\rho, T)$ and $a^{(r)}(\rho, T)$ the ideal and residual contributions to a, respectively. The former can be written as:

$$a^{(0)}(\rho, T) = a^{(0)}_{rr}(\rho, T) + a^{(0)}_{v}(\rho, T), \tag{5}$$

where subscripts rr and v refer to the rigid rotator and vibrational contributions to $a^{(0)}(\rho, T)$, respectively. As noted above, vibrational modes can be considered as frozen in the conditions under study, hence SF_6 thermodynamic properties have been obtained from a modified free energy expression, $\tilde{a}(\rho, T) = a^{(0)}_{rr}(\rho, T) + a^{(r)}(\rho, T)$ in which the vibrational contribution has been removed from the ideal part. The residual contribution has been left unchanged, since its expression, as is reasonable, does not contain any contribution which could be attributed to the different kinds of molecular degrees of freedom. As far as transport properties are concerned, lack of available data led to assign to μ_s, κ and μ_b

pressure independent values, respectively set to their known values at $T = 298$ K and 1 bar, listed below:

$$\mu_s = 1.52 \cdot 10^{-5} \ \frac{kg}{ms}, \quad \mu_b = 1.00 \cdot 10^{-5} \ \frac{kg}{ms}, \quad \kappa = 4.82 \cdot 10^{-3} \ \frac{W}{mK} \tag{6}$$

In absence of better alternatives, dense gas effects on the above quantities have been estimated by assuming that the dense rough spheres model [19] can be adopted to describe SF_6. Figure 2 shows the relative deviations of μ_s, μ_b and κ from their respective ideal gas limits, as a function of the reduced density η, for the values $0.2, 0.4, 0.6$ of the parameter $\kappa = \frac{4I}{m\sigma^2}$, where I is the molecular moment of inertia. The three curves show that in the interval $(0, 0.02)$, which includes the reduced density values relevant for this study, the largest deviation from the ideal value amounts to about 5% for μ_s and κ, a slightly larger dense gas effect is found for μ_s whose deviation amounts to about 8%. Therefore, theoretical spectra in the hydrodynamic regime have been obtained from three different lineshape models. The first one just adopts the ideal thermodynamic properties of SF_6 and the values of transport properties at 1 bar, given above. The second model introduces non-ideality only in thermodynamic properties, computing them from $\tilde{a}$ but keeping the values of transport properties fixed and equal to their respective values at 1 bar. The third model uses the same non-ideal thermodynamic properties of the second one but estimates dense gas effects on transport coefficients from the dense rough sphere model.

3. Kinetic modeling of fluctuations

Spectra of spontaneous fluctuations around equilibrium, in the collisionless and kinetic regime of dilute SF_6 have been obtained by DSMC simulations [8, 9, 10] of a gas of rigid rotors with 3 rotational degrees of freedom. The ideal gas behaviour is modelled by a standard DSMC implementation, where the total collision cross section is computed by the VSS collision model [16]. The Borgnakke-Larsen model [17], with a constant relaxation number, is adopted to describe energy exchange between translational and rotational degrees of freedom (particle selection prohibiting multiple relaxation [20]). Adopting the VSS model in place of the simpler Variable Hard Sphere (VHS) model [7] is crucial because the former allows obtaining both the correct gas viscosity and self-diffusion coefficients, the latter contributing to determine the correct gas thermal conductivity. On the contrary, VHS model parameters can only be tuned on viscosity. Accordingly, VSS model parameters have been chosen in order to reproduce recommended values of the shear viscosity, self-diffusion coefficient and rotational relaxation time. The exponent for the temperature dependence of the shear viscosity is taken from [14]. The adopted parameters setting is listed below:

- VSS diameter: $\sigma_{VSS} = 6.49 \cdot 10^{-10}$ m;
- VSS reference temperature: $T_{ref} = 298$ K;

- VSS temperature exponent: $\omega_{VSS} = 0.69$;
- VSS scattering angle parameter: $\alpha_{VSS} = 1.3$;
- Rotational relaxation number: $Z^{rot} = 5.66$.

3.1. Kinetic effects in the non-ideal regime

It is of some interest to complete the analysis of the kinetic regime by taking into account dense gas effects. At variance with the kinetic theory of dilute gases, the available theoretical tools to extend it to the dense gas regime are more limited and of more phenomenological nature [21]. Nevertheless, the extension of the classical Enskog theory of the dense hard sphere gas [22, 23], proposed in Ref. [24] to include the contribution of attractive intermolecular forces, can be considered a good starting point for the preliminary analysis presented below. In the present work, a straightforward extension of the so called Enskog-Vlasov (EV) equation [24] is considered to take into account rotational degrees of freedom, absent in the original formulation.
It is assumed that the gas consists of an assembly of identical molecules of mass m. The physical state of each molecule is characterized by its position in space $\boldsymbol{r}$, the velocity $\boldsymbol{v}$ of its center of mass and its angular velocity $\boldsymbol{\omega}$. Molecular interaction is split into an impulsive contribution, in the form of binary collisions and soft pairwise forces, derived from an attractive potential $\phi(r)$. Attractive forces act when the distance r between the centers of two molecules is larger than σ, the binary collision diameter. Under simplifying assumptions about pair correlations [25], a kinetic equation for the one-particle distribution function, $f(\boldsymbol{r}, \boldsymbol{v}, \boldsymbol{\omega}, t)$ can be derived, which in the spatially one-dimensional form needed here, takes the form [26, 27]:

$$\frac{\partial f}{\partial t} + v_x \frac{\partial f}{\partial x} + \frac{F_x\{n\}(x)}{m} \frac{\partial f}{\partial v_x} = C_E(f, f). \tag{7}$$

In Eq. (7), C_E denotes Enskog's collision integral [22]:

$$C_E(f,f) = \sigma^2 \int \left\{ \chi[n(x + \frac{\sigma k_x}{2})] f(x + \sigma k_x, \boldsymbol{\Gamma}_1^*) f(x, \boldsymbol{\Gamma}^*) \right. \\ \left. - \chi[n(x - \frac{\sigma k_x}{2})] f(x - \sigma k_x, \boldsymbol{\Gamma}_1) f(x, \boldsymbol{\Gamma}) \right\} (\boldsymbol{v}_r \cdot \hat{\boldsymbol{k}})^+ d\boldsymbol{\Gamma}_1 d^2\hat{\boldsymbol{k}} \tag{8}$$

where $\boldsymbol{\Gamma} = (\boldsymbol{v}, \boldsymbol{\omega})$ and $\chi(n)$ is the pair correlation function at contact of a hard sphere fluid in uniform equilibrium [21, 23]. In Eq. (8), the superscript $*$ denotes post-collision values. The rough sphere model [28] is assumed to govern the instantaneous collisions dynamics:

$$\boldsymbol{v}^* = \boldsymbol{v} + (\boldsymbol{W} \cdot \hat{\boldsymbol{k}})\hat{\boldsymbol{k}} + \theta \boldsymbol{W}_t, \qquad \boldsymbol{\omega}^* = \boldsymbol{\omega} - \frac{m\sigma}{2I}\theta(\hat{\boldsymbol{k}} \wedge \boldsymbol{W}), \tag{9}$$

$$\boldsymbol{v}_1^* = \boldsymbol{v}_1 - (\boldsymbol{W} \cdot \hat{\boldsymbol{k}})\hat{\boldsymbol{k}} - \theta \boldsymbol{W}_t, \qquad \boldsymbol{\omega}_1^* = \boldsymbol{\omega}_1 - \frac{m\sigma}{2I}\theta(\hat{\boldsymbol{k}} \wedge \boldsymbol{W}). \tag{10}$$

In the above expressions, $\boldsymbol{W}$ is the relative velocity at the contact point of the two colliding spheres:

$$\boldsymbol{W} = \boldsymbol{v}_1 - \boldsymbol{v} + \frac{\sigma}{2}(\boldsymbol{\omega} + \boldsymbol{\omega}_1) \wedge \hat{\boldsymbol{k}}, \tag{11}$$

whereas $\boldsymbol{W}_t$ is the component of $\boldsymbol{W}$ in the plane normal to $\hat{\boldsymbol{k}}$, the unit vector along the line connecting the centres of the spheres at the time of their impact. The coefficient θ is defined as $\theta = \kappa(1+\beta)/(2+2\kappa)$, being κ the normalized molecular moment of inertia defined in Section 2.
The non-dimensional parameter β allows to switch from smooth to perfectly rough spheres collision dynamics. More precisely one has:

1. $\beta = 1$, $\boldsymbol{W}^* = -\boldsymbol{W}$, perfectly rough spheres;
2. $\beta = -1$, $\boldsymbol{W}_t^* = \boldsymbol{W}_t$, smooth spheres: the rotational dynamics is decoupled from the translational one.

A finite rotational relaxation time is obtained from the model above, requiring that $\beta = 1$ with probability P^{rot} or $\beta = -1$ with probability $1 - P^{rot}$.
In the EV approximation, attractive forces appear in Eq. (7) through the self-consistent force field $F_x\{n\}(x,t)$, defined below as a linear functional of the number density n:

$$F_x(x,t) = -2\pi \left[\phi(\sigma) \int_{|y-x|\leq\sigma} (y-x) n(y,t)\, dy + \int_{|y-x|>\sigma} (y-x)\phi(|y-x|) n(y,t)\, dy \right]. \tag{12}$$

It is easily shown that uniform equilibrium solutions of the EV equations lead to the following expressions for the pressure equation of state $p(n,T)$ and the specific internal energy $u(n,T)$:

$$p(n,T) = = nk_bT\left[1 + \frac{2\pi}{3}a^3 n\chi(n)\right] - \alpha_p n^2, \tag{13}$$

$$u(n,T) = 6k_bT - \alpha_u n, \tag{14}$$

where α_p and α_u are two constants whose values depend on $\phi(r)$. Although it would be possible to determine $\chi(n)$ from Eq. (13) and experimental SF_6 isotherms [21], the classical expression, derived from the Carnahan-Starling [29] equation of state for the hard sphere fluid has been used, for simplicity. Accordingly:

$$\chi(n) = \frac{1}{2}\frac{2-\eta}{(1-\eta)^3} \tag{15}$$

Moreover, $\phi(r)$ has been set equal to the attractive contribution of the classical Lennard-Jones $12-6$ potential:

$$\phi(r) = -\phi_\sigma \left(\frac{\sigma}{r}\right)^6, \quad r > \sigma, \tag{16}$$

for which one has $\alpha_p = \frac{4\pi}{3}\sigma^3\phi_\sigma$ and $\alpha_u = \alpha_p/2$.
The particular form of the EV equation adopted here is based on the so called SET (Standard Enskog Theory) of dense gases. SET assumes that the pair correlation function at contact [21] is approximated by its uniform equilibrium form, $\chi(n)$, evaluated at the contact point of two colliding spheres. SET has the advantage of simplicity but a number of drawbacks, lacking the proof of an H-theorem and its multi-component version being not compatible with the thermodynamics of irreversible processes. Further studies have corrected SET deficiencies by modifications of varying complexity [30, 31, 32]. However, it should be noted that previous studies of strongly non-uniform flows of the dense hard sphere fluid have shown that SET is able to reproduce extremely well "exact" results from deterministic molecular dynamics simulations [33, 34], in spite of its simplicity.

Transport properties of the EV fluid are determined solely by the collision term [25]. As a result, the transport coefficients coincide with those of the dense rough sphere fluid, determined in Ref. [19].
As is clear from the model setting described above, the properties of the EV fluid are determined by the following physical parameters:

- Individual molecular properties: m, σ, κ.
- Molecular interaction properties: ϕ_σ, P^{rot}

With the obvious exception of the molecular mass, the four remaining parameters have been obtained by fitting the analytical *hydrodynamic* EV spectra to the experimental ones at 5 bar. Among the different data setting, providing a comparable level of approximation, further selection has been made, based on the accuracy of thermodynamic quantities at $T = 298$ K and $p = 5$ bar. The fitting provided the following parameters setting:

- $\sigma_{EV} = 6.63 \cdot 10^{-10}$ m;
- $\phi_{EV} = 237$ K;
- $\kappa = 0.67$;
- $P_{rot} = 0.5$.

The values listed above have been used to obtain fluctuation spectra in all pressure conditions, by the DSMC extension to dense fluids described in Refs. [35, 26]. In principle, fluctuations spectra of the EV equation could be obtained from its linearized form or from some extended form of hydrodynamic equations, in order to describe kinetic effects. For the Enskog equation (*i.e.* hard sphere fluid, without the mean field contribution), Grad's 13 moments approximation and linearized hydrodynamic equations to the Burnett order have been obtained in

Refs. [36, 37]. Both approximations have been applied to study the propagation of sound waves. More recently, Grad's 13 moments equations for the full EV equation have been obtained in Ref. [38]. Although all approximations mentioned above could be used to study fluctuation spectra in a dense fluid, both in the hydrodynamic and kinetic regime (to some extent), they are restricted to monatomic gases. Unfortunately, their extension to the polyatomic gas model considered here is feasible but far from trivial. The DSMC approach is more viable, although much more computationally expensive.
In view of the EV results presentation and discussion given below, it should be noted that the matching of the EV model to the SF_6 physical properties has not been as sophisticated as it could have been [39]. As explained above, repulsive forces have been modeled by the dense hard sphere fluid pair correlation function, whereas a very specific attractive soft potential tail has been used. In principle, both $\chi(n)$ and $\phi(r)$ could have been better taylored on the SF_6 pressure equation of state [21]. However, in view of the exploratory character of the EV model described here, it has been decided to reduce the model flexibility in favor of a simpler fitting procedure.

4. Results

This section is devoted to the presentation of the theoretical fluctuations spectra obtained from the models described above and to their comparisons with experimental data, described in [11] along with a kinetic and hydrodynamic ideal gas models analysis. For each experimental spectrum, an accuracy figure can be obtained from the asymmetry in the measured spectrum at corresponding negative and positive frequencies. Additionally, for pressures of 1 bar and above, two spectra have been measured at practically identical conditions. The difference between the two provides an estimate of the experimental accuracy, found to be of the order of a few percent of the peak value (5% for the worst case at $p = 5$ bar). The main result of that study is provided in fig. 3 of ref. [11]. While it is expected that the hydrodynamic prediction fails at low pressure, all models show a worsening of their predictions with increasing pressure, which suggested that dense-gas effects might be playing a role [11].

Comparisons between experiments and theoretical spectra from the present work have been based on the following procedure: simulated spectra are first convoluted with the instrument function as described in [11] and then normalised such that the integral over the prescribed frequency range is unity:

$$2\int_0^{f_M} S(f)df = 1. \tag{17}$$

The frequency upper bound, $f_M = 3.73\ GHz$, is the same as in the experiment. When comparing to the experimental spectra, measured at frequencies (f_i, $i = 1, N$), the differences are measured in terms of the normalised root-mean square

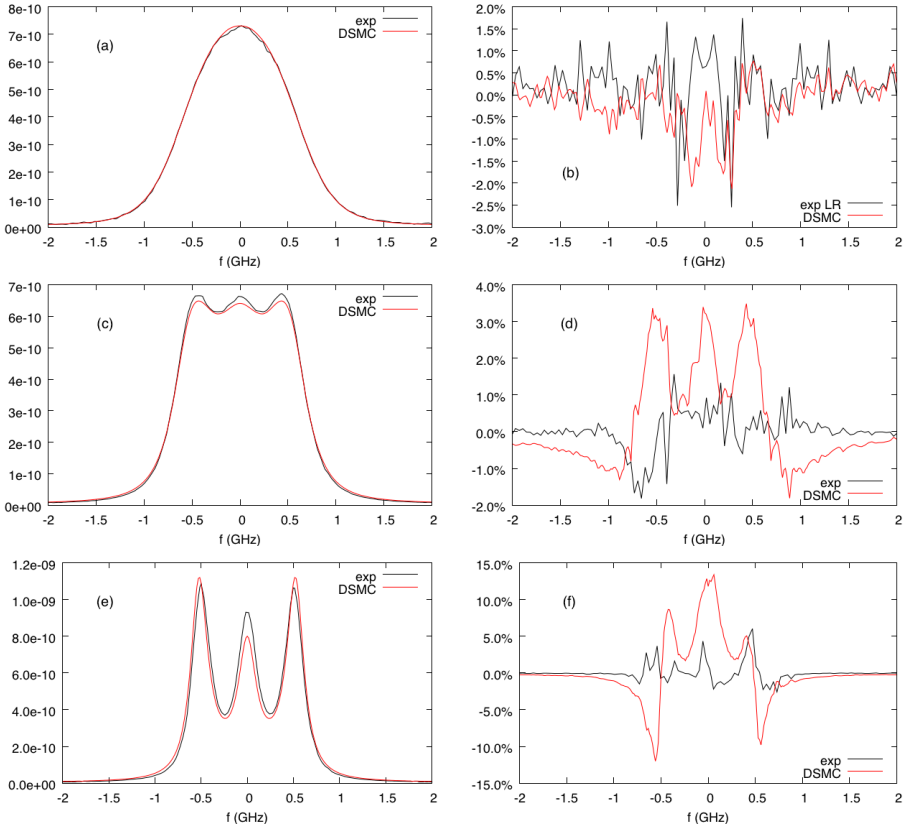

Figure 3: Comparisons of experiment and DSMC spectra for three experimental conditions. From top to bottom: $p = 0.2, 1.0, 5.0$ bar. Panels on the left compare experimental and computed normalized spectra; panels on the right compare the relative difference between simulation and experiment (the *simulation error*) with the estimated experimental accuracy.

deviation defined by:

$$\Sigma_{nRMS} = \sqrt{\frac{1}{N}\sum_{i=1}^{N}\left(S_e(f_i) - S_s(f_i)\right)^2}, \tag{18}$$

where S_e and S_s are the experimental and simulated spectra, respectively, and $N = 200$. Σ_{nRMS} is expressed as a fraction of the maximum of the experimental spectrum.

4.1. Ideal gas models and rarefied-gas effects

Figure 3 shows the comparisons between the light scattering spectra obtained from DSMC simulations at three experimental conditions and the corresponding measurements. DSMC can successfully match the experimental results at

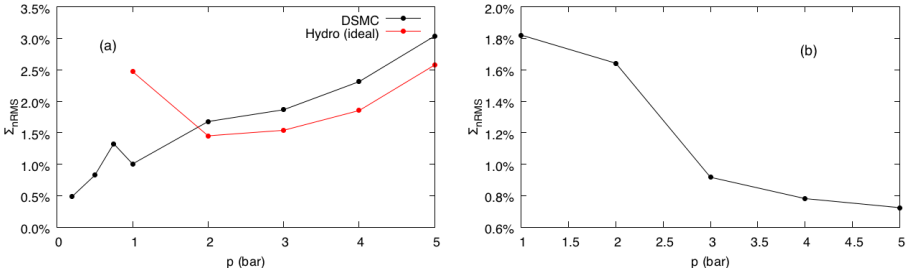

Figure 4: **(a)** Root-mean square deviations Σ_{nRMS} normalised by the spectrum peak value, as obtained from comparison between DSMC and Hydrodynamic (ideal gas) spectra with the experiment. **(b)** Root-mean square deviations Σ_{nRMS} normalised by the spectrum peak value, as obtained from comparison between DSMC and Hydrodynamic spectra with an ideal gas EoS.

the low pressures: the differences between simulation and experiment, expressed as a fraction of the experimental spectrum peak value, are comparable to the measurements accuracy, here estimated by the left-right asymmetry of experimental spectra (Fig. 3b). With increasing pressure, deviations increase, thus supporting the hypothesis of an increasing role of dense-gas effects. In particular, the comparison of the 5 bar spectra (Figs. 3e-f) suggests that the major causes of the discrepancy are incorrect specific heats (that control the Rayleigh to Brillouin area ratio) and speed of sound (that controls the position of the Brillouin peaks). The widths of the peaks, instead, that are determined by the transport properties, are fairly well reproduced keeping the 1 bar values of the SF_6 transport coefficients unchanged while increasing p.
Hydrodynamic spectra obtained by the ideal gas model are therefore expected to fail both at low pressure, where the hydrodynamic regime is not attained, and at high pressure where dense-gas effects are noticeable. This is indeed the case and Fig. 4a reports a summary of the results obtained with the ideal gas model. Comparison of results from the two models can also give indications about the extent of rarefied-gas (or kinetic) effects. When the experiment is in the hydrodynamic regime, then the two spectra shall coincide. Figure 4b summarizes the RMS deviation between the two models as a function of pressure. It can be concluded that a purely hydrodynamic regime is obtained for $p = 3$ bar or larger.

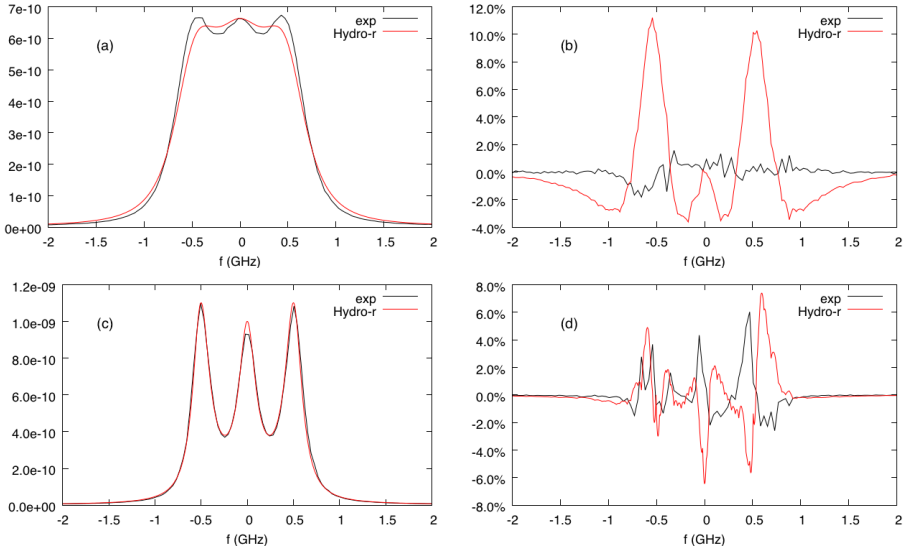

Figure 5: Comparisons of experiment and Hydrodynamic (dense gas) spectra for $p = 1$ bar (a,b) and $p = 5$ bar (c,d). Panels on the left compare experimental and computed normalized spectra; panels on the right compare the relative difference between simulation and experiment (the *simulation error*) with the estimated experimental accuracy.

4.2. Dense-gas Effects

Results for the hydrodynamic model that includes density-dependent perturbations to the ideal gas EoS are reported in Fig. 5. The model successfully reproduces the experimental spectrum at 5 bar. This confirms that dense-gas corrections are indeed required in order to understand the experimental results. The model, however, cannot reproduce the experimental results at lower pressures where rarefied-gas effects, not captured by the hydrodynamic formulation, play a role. The differences between the spectra obtained with this model and the experiment are summarised in Fig. 6a. Dense-gas effects can be estimated by comparing the spectra obtained with the hydrodynamic models with the ideal gas and dense gas equations of state, respectively. Results are reported in Fig. 6b. Dense-gas effects result in differences between the spectra that increase with pressure. At $p = 2$ bar, the differences are already larger than the experimental accuracy ($\approx 1\%$) and therefore measurable.

The theoretical spectra displayed in Fig. 5 have been obtained keeping the SF_6 transport coefficients fixed to their values at $T = 298$ K and $p = 1$ bar, as given by Eqs (6). Thermodynamic properties have been changed according to the REFPROP data mentioned in Section 2. Dense gas effects on transport properties have been estimated by assuming that the density dependence of SF_6 transport coefficients can be obtained by the rough sphere model [19]. Accordingly, new spectra have been computed correcting SF_6 transport coefficients at $T = 298$ K and $p = 1$ bar by the factors $\Delta\mu_s$, $\Delta\mu_b$ and $\Delta\kappa$ at $\eta = 0.02$ (See Fig. 2). Applied corrections cause a 5% increase of μ_s and κ and an 8% increase

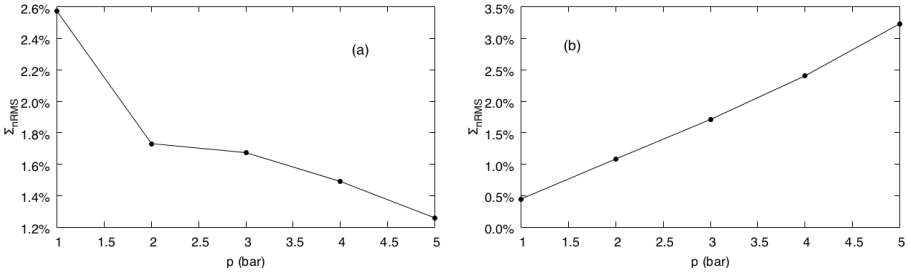

Figure 6: **(a)** Root-mean square deviations Σ_{nRMS} normalised by the spectrum peak value, as obtained from comparison between Hydrodynamic (dense gas) spectra with the experiment. **(b)** Root-mean square deviations Σ_{nRMS} normalised by the spectrum peak value, as obtained from comparison between Hydrodynamic spectra from ideal and dense gas EoS.

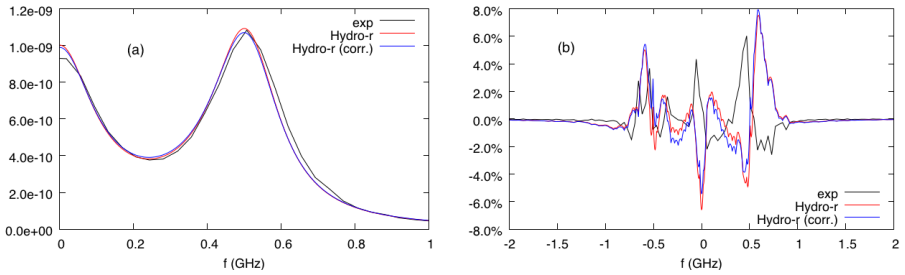

Figure 7: **(a)** Effect of estimated dense gas correction on SF_6 spectrum at $p = 5$ bar: Experimental data (black solid line); Hydrodynamic spectrum from SF_6 transport coefficients values at $p = 5$ bar (red solid line); Hydrodynamic spectrum from SF_6 transport coefficients with dense gas corrections from dense rough sphere gas (blue solid line). **(b)** Errors of computed spectra from experimental data, compared to experimental error. Errors are expressed as a fraction of the experimental spectrum peak value. Line marking is the same as above.

of μ_b. As shown in Fig. (7), the transport coefficient corrections do not change the spectra appreciably, suggesting that thermodynamic properties are mainly responsible of dense gas effects on spectra, in the considered pressure range.

4.3. EV results

In the previous sections, we have shown that experimental spectra can be reproduced at low pressure by DSMC simulations and at high pressures by a hydrodynamic model accounting for dense-gas perturbations to the thermodynamic properties, as expected. It is of interest to explore the possibility that an intermediate regime exists where the Boltzmann equation ceases to work because of the onset of dense gas effects but hydrodynamics is not yet accurate enough, due to the persistence of kinetic effects. To this purpose, DSMC simulations, based on the Enskog-Vlasov model formulation described in Section 3.1, have been performed to obtain fluctuations spectra to be compared with experimental ones at different pressures. Particular care has been taken to select the computational parameters affecting the calculation of the mean field, given by Eq. (12), in order to prevent systematic numerical errors in the energy conservation. It should be noted that energy is conserved to machine precision by the DSMC collision algorithm, both in the ideal and dense versions. In the EV equation, the mean field term is the result of pair interactions through opposite forces depending only on particles relative positions (see Eq. (12)). Although energy is conserved in the mathematical model, deviations, in the form of small system temperature drifts from the imposed equilibrium values, are observed as a result of the space and time discretization of the free flight DSMC step. Such systematic errors are kept within acceptable limits (well below 1%, in this work) by suitable choices for the integration time step and the size of the grid used to compute the mean field.

Figure 8 shows the results for three pressures, whereas fig. 9 summarizes the overall deviations from the experimental data as a function of pressure. It is immediately seen from the 0.2 bar spectra that EV correctly reproduces the nearly free molecular limit, as the ideal gas DSMC does.

As a result of the EV parameter identification, based on the best fitting of the 5 bar spectra, the agreement is quite good, particularly on the Brillouin peaks. The discrepancy on the central peak is probably exaggerated by the unavailability of the experimental zero frequency value. The relative error of the spectrum at 1.0 bar is comparable in magnitude. In this regime, the EV fluid behaves as an ideal hard sphere gas and its predictions should be close to those of the ideal gas DSMC presented in Section 4.1. The comparison of the EV 1.0 bar spectrum on Fig. 8 with the corresponding ideal gas counterpart on Fig. 3 shows that the two models predict similar spectra, at this pressure. The ideal gas DSMC exhibit a lower error but it should be noted that the two kinetic models are based on different collision cross sections whose different fittings do not guarantee identity of results. Figure 9 summarizes the root-mean square deviations of the EV predictions from experiments. Although the error, which probably reflects the inadequacy of the present model setting as far as fine tuning of SF_6 properties is concerned, remains larger than the experimental one, it is to be noted that it stays bounded over the whole pressure range.

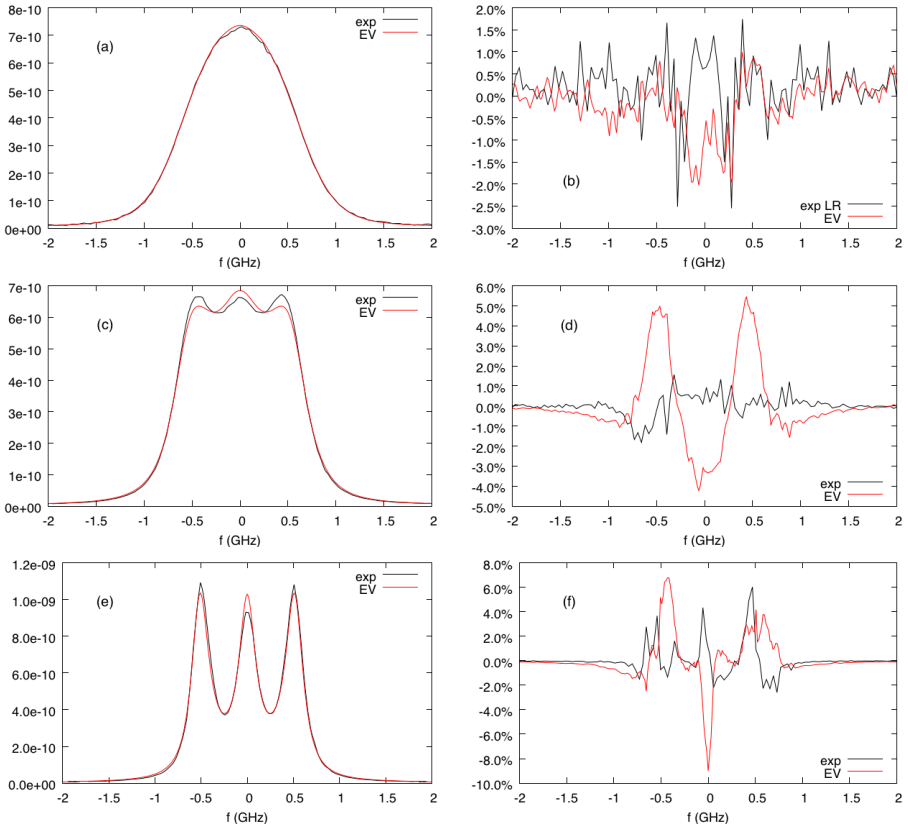

Figure 8: Comparison of experimental and DSMC-EV spectra for $p = 0.2, 1.0, 5.0$ bar. Lower pressure data on top graphs.

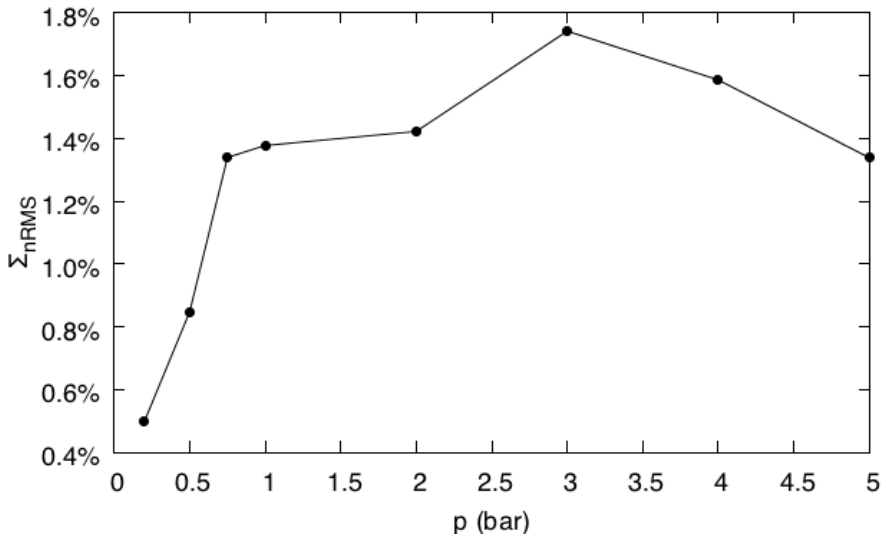

Figure 9: Root-mean square deviations Σ_{nRMS} normalised by the spectrum peak value, as obtained from comparison between DSMC-EV spectra with the experiment.

5. Summary and conclusions

Figure 10 summarizes the results obtained in this study in terms of the RMS deviation to the experimental results as a function of pressure, from the kinetic and hydrodynamic models; the estimated experimental accuracy is also reported for comparison. A perfect agreement is only found in the trivial col-

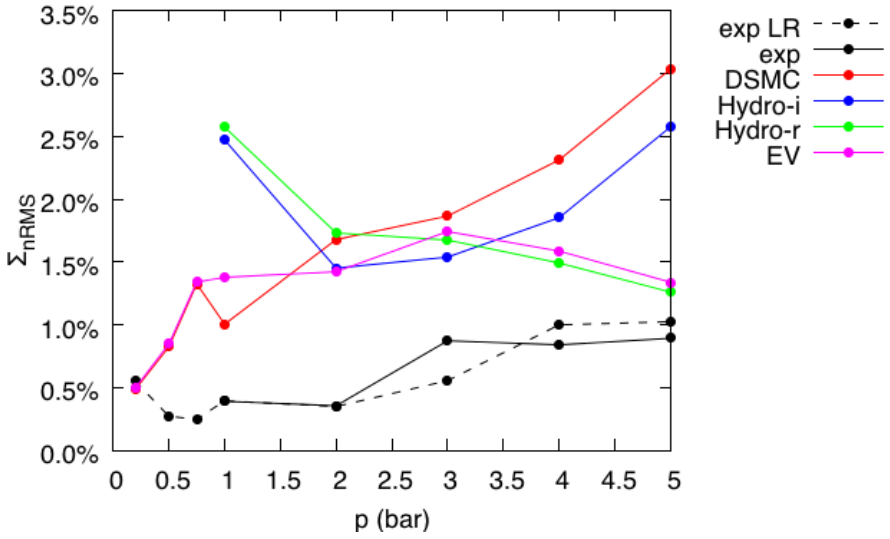

Figure 10: Normalized root-mean square deviations Σ_{nRMS} normalised by the spectrum peak value, as obtained from comparison between experimental spectra and the various line shape models used in this study. The estimated experimental accuracy is also reported for comparison.

lisionless regime, yet some conclusions may be drawn. The first one is the substantial improvement of theoretical predictions when dense gas thermodynamics is adopted into the hydrodynamic description of SF_6 at high pressure. Actually, even if deviations from the ideal gas EoS are only few percent at the largest pressure, their effect can clearly be resolved given the large accuracy of the experiment. As shown in Fig. 10, models including dense gas effects perform definitely better than ideal gas based models for $p > 3$ bar. In the kinetic regime, whose upper limit can be placed at $p \approx 2$ bar, both the ideal gas DSMC and EV produce predictions of comparable quality. Between 2 and 3 bar, the predictions of all models fall within $1.5 - 2.0\%$ from experimental data and, although the high pressure trend is clear, it is difficult here to tell kinetic/dense effect apart and make a clear distinction. Finally, it is observed that the particular implementation of the Enskog-Vlasov model adopted here allows a good prediction of experimental spectra across the whole pressure range.

6. Acknowledgments

The authors wish to thank W. Ubachs for providing the experimental data.

[1] J. P. Boon and S. Yip, *Molecular Hydrodynamics* (Dover Books on Physics, 1980).

[2] M. O. Vieitez, E. J. van Duijn, W. Ubachs, B. Witschas, A. Meijer, A. S. de Wijn, N. J. Dam, and W. van de Water, Phys. Rev. A **82**, p. 043836 (2010).

[3] M. M. Mansour, A. L. Garcia, G. C. Lie, and E. Clementi, Phys. Rev. Lett. **58**, 874–877 (1987).

[4] J. M. O. de Zárate and J. V. Sengers, *Hydrodynamic Fluctuations in Fluids and Fluid Mixtures* (Elsevier Science, 2006).

[5] C. Cercignani, *The Boltzmann Equation and Its Applications* (Springer-Verlag, Berlin, 1988).

[6] G. Tenti, C. Boley, and R. Desai, Can. J. Phys. **52**, p. 285 (1974).

[7] G. A. Bird, *Molecular Gas Dynamics and the Direct Simulation of Gas Flows* (Clarendon Press, Oxford, 1994).

[8] D. Bruno, M. Capitelli, S. Longo, and P. Minelli, Chem. Phys. Lett. **422**, 571–574 (2006).

[9] D. Bruno, A. Frezzotti, and G. P. Ghiroldi, Phys. Fluids **27**, p. 057101 (2015).

[10] D. Bruno, A. Frezzotti, and G. P. Ghiroldi, Eur. J. Mech. B/Fluids **64**, 8–16 (2017).

[11] Y. Wang, Y. Yu, K. Liang, W. Marques, W. van de Water, and W. Ubachs, Chem. Phys. Lett. **669**, 137–142 (2017).

[12] W. Marques Jr, Physica A **264**, 40–51 (1999).

[13] E. W. Lemmon, M. L. Huber, and M. O. McLinden, NIST Standard Reference Database 23: Reference Fluid Thermodynamic and Transport Properties-REFPROP, Version 8.0, National Institute of Standards and Technology, 2007.

[14] C. Tantos, G. P. Ghiroldi, D. Valougeorgis, and A. Frezzotti, Int. J. Heat Mass Transf. **102**, 162–173 (2016).

[15] E.-U. Haebel, Acta Acust. united Ac. **20**, 65–75 (1968).

[16] K. Koura and H. Matsumoto, Phys. Fluids **3**, 2459–2465 (1991).

[17] C. Borgnakke and P. S. Larsen, J. Comput. Phys. **18**, 405–420 (1975).

[18] C. Guder and W. Wagner, J. Phys. Chem. Ref. Data **38**, 33–94 (2009).

[19] B. J. McCoy, S. I. Sandler, and J. S. Dahler, J. Chem. Phys. **45**, 3485–3512 (1966).

[20] B. L. Haas, D. B. Hash, G. A. Bird, F. E. L. III, and H. A. Hassan, Phys. Fluids **6**, p. 2191 (1994).

[21] P. Resibois and M. DeLeener, *Classical Kinetic Theory of Fluids* (J. Wiley & Sons, New York, 1977).

[22] D. Enskog, Kungl. Svenska Vet.-Ak. Handl. **63**, p. 3 (1922).

[23] H. van Beijeren and M. H. Ernst, Physica **68**, p. 437 (1973).

[24] L. de Sobrino, Can. J. Phys. **45**, 363–385 (1967).

[25] J. Karkheck and G. Stell, J. Chem. Phys. **75**, 1475–1487 (1981).

[26] A. Frezzotti, L. Gibelli, and S. Lorenzani, Phys. Fluids **17**, p. 012102 (2005).

[27] M. Kon, K. Kobayashi, and M. Watanabe, Phys. Fluids **26**, p. 072003 (2014).

[28] S. Chapman and T. G. Cowling, *The Mathematical Theory of Non-Uniform Gases* (Cambridge University Press, 1995).

[29] N. F. Carnahan and K. E. Starling, J. Chem. Phys. **51**, p. 635 (1969).

[30] H. V. Beijeren and M. H. Ernst, Physica **68**, 437–456 (1973).

[31] P. Resibois, J. Stat. Phys. **19**, 593–609 (1978).

[32] E. S. Benilov and M. S. Benilov, Phys. Rev. E **97**, p. 062115 (2018).

[33] A. Frezzotti, Comput. Math. Appl. **35**, 103–112 (1998).

[34] A. Frezzotti, Eur. J. Mech. B/Fluids **18**, 103–119 (1999).

[35] A. Frezzotti, Phys. Fluids **9**, 1329–1335 (1997).

[36] G. M. Kremer and E. Rosa Jr., J. Chem. Phys. **89**, 3240–3247 (1988).

[37] W. Marques Jr and G. M. Kremer, Rev. Bras. Fis. **21**, 402–417 (1991).

[38] H. Struchtrup and A. Frezzotti, "Grad's 13 moments approximation for Enskog-Vlasov equation," in *Proceedings of the* 31^{st} *International Symposium on Rarefied Gas Dynamics*, AIP Conference Proceedings, edited by Y. Zhang, J. Reese, and D. Lockerby (Glasgow, UK, 2019) to appear.

[39] E. S. Benilov and M. S. Benilov, Phys. Rev. E **99**, p. 012144 (2019).